Thin Solid Films 519 (2011) 6369–6373

Contents lists available at ScienceDirect

Thin Solid Films

journal homepage: www.elsevier.com/locate/tsf

# Interpretation of the two-components observed in high resolution X-ray diffraction ω scan peaks for mosaic ZnO thin films grown on c-sapphire substrates using pulsed laser deposition

O. Durand [a,*], A. Letoublon [a], D.J. Rogers [b,c], F. Hosseini Teherani [b]

[a] Université Européenne de Bretagne, INSA, FOTON, UMR 6082, 20 avenue des Buttes de Coësmes, F-35708 RENNES, France
[b] Nanovation SARL, 103 bis rue de Versailles, 91400 Orsay, France
[c] SUPA, School of Physics and Astronomy, University of St. Andrews, St. Andrews, KY16 9SS, UK

ARTICLE INFO

*Article history:*
Received 30 August 2010
Received in revised form 3 January 2011
Accepted 10 April 2011
Available online 16 April 2011

*Keywords:*
Zinc oxide
Thin films
X-ray scattering
Transverse scans
Misfit dislocations
Heteroepitaxy

ABSTRACT

X-ray scattering methods were applied to the study of thin mosaic ZnO layers deposited on c-$Al_2O_3$ substrates using Pulsed Laser Deposition. High Resolution (HR) studies revealed two components in the ω scans (transverse scans) which were not resolved in conventional "open-detector" ω rocking curves: a narrow, resolution-limited, peak, characteristic of long-range correlation, and a broad peak, attributed to defect-related diffuse-scattering inducing a limited transverse structural correlation length. Thus, for such mosaic films, the conventional ω rocking curve Full Width at Half Maximum linewidth was found to be ill-adapted as an overall figure-of-merit for the structural quality, in that the different contributions were not meaningfully represented. A "Williamson-Hall like" integral breadth (IB) metric for the HR (00.l) transverse-scans was thus developed as a reliable, fast, accurate and robust alternative to the rocking curve linewidth for routine non-destructive testing of such mosaic thin films. For a typical ZnO/c-$Al_2O_3$ film, the IB method gave a limited structural correlation length of 110 nm ± 9 nm. The results are coherent with a thin film containing misfit dislocations at the film-substrate interface.



## 1. Introduction

Wurtzite zinc oxide (ZnO) is a remarkable multifunctional material with a wide range of established and emerging applications [1,2]. These include a variety of optoelectronic uses based on a distinctive combination of properties such as a direct wide bandgap (3.37 eV), relatively high exciton binding energy (60 meV), good transparency over the whole visible spectrum and a conductivity which can be readily tuned from semi-insulating to semi-metallic [3–8].

Since large area ZnO substrates are not yet available at a reasonable cost level, there is currently a need to grow ZnO on alternative substrates. The most widely adopted choice, for opto-electronic applications, is c-sapphire (c-$Al_2O_3$). Although, there are significant lattice and thermal mismatches [9], ZnO is a relatively compliant material [10], and it can be grown on c-$Al_2O_3$ in the form of epitaxial "blocks" with rotational misorientation (or "tilt") relative to one another. These monocrystalline or "mosaic" blocks scatter X-rays incoherently with respect to each other [11,12].

The most widely adopted metric for the comparison of the crystal quality for such films is the full-width at half maximum (FWHM) (or linewidth) of the (00.2) peak of the X-ray diffraction (XRD) "rocking-curve." However, this metric can be misleading in the characterisation of a thin film with such a mosaic structure. First of all, this is because this metric strongly depends on the experimental conditions, since, in the literature, the term "rocking-curve" is often used, confusingly, to refer not only to the conventional "open-detector" scan but also to the high resolution, HR, ω-scan experiments performed with "channel-cut" optics in the diffracted-beam path ("transverse scans"). In the case of epitaxial thin films, XRD ω-scan experiments should, ideally, be done with such a channel-cut in the diffracted beam path in order to differentiate contributions orthogonal and parallel to the sample surface. Indeed, the relatively low thickness of these ZnO layers in itself generates a widening of the diffraction peak, orthogonal to the sample surface. This is due to the presence of "crystal truncation rods", which resemble, but have nothing to do with, a defect-induced effect. Secondly, since the peak broadening has multiple origins, differentiation of these causes is desireable in order to compare samples. In this paper, we report on the development of a rapid, robust and reliable alternative to the conventional ω rocking curve figure-of-merit, which is better adapted for the characterisation of such mosaic thin films and which can be

* Corresponding author. Tel.: +33 2 23 23 86 28; fax: +33 2 23 23 86 18.
*E-mail address:* olivier.durand@insa-rennes.fr (O. Durand).

0040-6090/$ – see front matter © 2011 Elsevier B.V. All rights reserved.
doi:10.1016/j.tsf.2011.04.036

readily extracted from the XRD transverse-scans. Moreover, the present method is applicable to other thin "mosaic-block" material systems, e.g. (00.*l*)-oriented wurtzite materials (such as GaN) and (00*l*)-oriented zinc-blende materials (such as GaP, InAs, etc.).

## 2. Experimental details

ZnO thin films were grown on c-$Al_2O_3$ substrates held at elevated substrate temperature in a home-made Pulsed Laser Deposition (PLD) system using a Coherent KrF excimer laser (248 nm) [13]. The laser spot was focused onto a 5 N sintered target to give a fluence of up to about 4 J/cm$^2$. During the growth, various parameters were adjusted in order to maintain a 2D growth. In particular pulse repetition rate was varied between 1 and 50 Hz and molecular oxygen ($O_2$) background pressure was varied between $1.3\times10^{-4}$ and $1.3\times10^{-1}$ Pa. HRXRD and Very HRXRD (VHRXRD) experiments were conducted in Panalytical MRD-Pro and Seifert PTS systems, respectively. For both, a $Cu_{K\alpha1}$ source ($\lambda=0.15406$ nm) with line focus was adopted. The HR and VHR experiments were carried out using four-bounce Ge (220) and (440) crystal monochromators in the incident-beam path, giving incident-beam divergences of 12 and 5 arcsecs and wavelength dispersions ($\frac{\Delta\lambda}{\lambda}$) as low as $1.4\times10^{-4}$ and $5.5\times10^{-5}$, respectively. A multilayer mirror was employed to enhance the incident intensity. Two incremental encoders allowed an angle reading to an accuracy of $+0.0002°$ for both the ω and 2θ positions. The HR and VHR XRD were performed, respectively, with two-bounce Ge (220) and (440) channel-cut crystals in the diffracted-beam path, giving detector acceptance angles of 12 and 5 arcsecs, respectively (i.e. 0.0033° and 0.0014°). For X-ray Reflectometry (XRR), the measurements were performed using a detector slit of 0.1 mm with back Soller slits and a knife-edge located at 60 μm from the sample surface, so as to reduce the background signal to 0.05 counts per second. Thus, a dynamic intensity range of $10^7$ could be achieved for the reflectivity curves.

Two scan modes were employed: ω/2θ scans which provided information on crystal planes parallel to the sample surface, and ω rocking-curves (rotation of the sample around the ω axis, while keeping the detector at a fixed 2θ), which gave the dispersion in the orientation of the crystal planes for a given lattice spacing, plus information on the in-plane correlation lengths. In the following, we will refer to the HR version of the ω rocking-curves (performed with a channel-cut crystal in the diffracted beam path) as "transverse-scans".

The process of deconvoluting multicomponent peaks such as those observed for mosaic thin films is usually carried out using either the Fourier technique [14] or the variance method [15,16] plus direct modelling [17,18] of the diffraction-peak profiles. Fast analysis of the peak breadths [19], called the Integral-Breadth (IB) method, is adequate for practical purposes, however, when an estimation of the coherent domain size (termed "crystallite size") is required, even if this method tends to overestimate the domain size value when compared with alternative methods [20]. It should be noted that the IB, defined as the width of a rectangle having the same area and height as the observed line profile, has already been put forward as a more useful metric than the FWHM [21]. It is well-known, for instance, that the broadening of the (00.*l*) reflections in the ω/2θ mode can be used to estimate the correlation length of the diffraction domains (coherent domain size) in the growth direction, after separating both the strain and the correlation length components responsible for the IB widening, through the Halder and Wagner parabolic approach [22], a variant of the Williamson–Hall plots method. In particular, when considering the ZnO epitaxial thin films investigated in the present paper, the growth-direction coherent-domain-size has been found [23] to be comparable with the layer thickness (determined by XRR) bringing to the fore the high-crystalline-quality in the growth direction. Then, any overall measurement of the structural quality will include a contribution from in-plane defects. Thus, an appropriate "figure-of-merit" needs to be incorporate both the lateral correlation length and the mosaicity. We propose a method for this, in the following, based on a line-profile analysis of (00.*l*) XRD transverse-scans, through an IB approach. This can then be used as a reliable metric for comparing the structural quality of thin ZnO layers grown on c-$Al_2O_3$ substrates.

The interpretation of the results is facilitated by considering reciprocal space co-ordinates, which are related to the angular space co-ordinates by the following relationships:

$$S_x = \frac{2}{\lambda}\sin\theta\ \sin(\omega-\theta) \tag{1}$$

$$S_z = \frac{2\ \sin\theta}{\lambda} \tag{2}$$

where $S_x$ and $S_z$ are the diffraction vector along the sample surface and perpendicular to the sample surface, respectively (assuming that the diffraction planes are parallel to the sample surface, i.e. $\omega=\theta$). Therefore, the angular-space IBs $\beta(2\theta)$, from a ω/2θ scan, and $\beta(\omega)$, from a transverse scan, can be translated into reciprocal space coordinates of the variables $S_x$ and $S_z$ by the following relationships:

$$\beta_z(S) = \beta(2\theta)\frac{\cos\theta}{\lambda} \tag{3}$$

$$\beta_x(S) = \beta(\omega)\frac{2\ \sin\theta}{\lambda} \tag{4}$$

A process of deconvolution to allow for the instrumental profile was also carried out, as described elsewhere [23]. In the following, β refers to the instrument-corrected IB.

## 3. Results and discussion

Fig. 1 shows an XRR scan for a typical ZnO layer grown on a c-$Al_2O_3$ substrate. The Auto-Correlation Function (ACF) obtained through a Fourier transform of the XRR profile (corrected for refraction [24]) displays a peak centered at 178.1 nm ± 0.2 nm The thickness fringes could be followed up to an $S_Z$ value as large as 0.55 nm$^{-1}$, indicating that both the film-air and film-substrate interfaces were relatively flat. In complement to the XRR, specular ω/2θ XRD analyses were performed around the (00.2) Bragg reflection, as shown in Fig. 2. The thickness fringes, in this case, extend up to 0.35 nm$^{-1}$ around the Bragg peak indicating that the ZnO displays excellent crystalline quality over the thickness corresponding to the correlation length indicated by the fringes. The fringe spacing gives a correlation length of 177.5 nm ± 0.2 nm, which is very close to the thickness determined by XRR. Therefore, the entire film is scattering in phase, which shows that the crystalline quality is quasi-perfect along the growth direction.

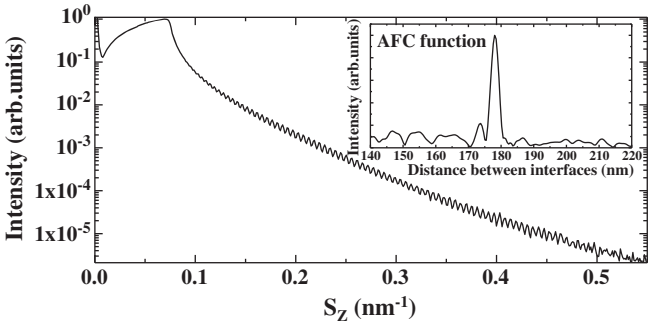


**Fig. 1.** An XRR scan for a ZnO thin film grown on c-$Al_2O_3$. Inset: ACF obtained from the XRR profile, corrected for refraction and normalised to the substrate Fresnel reflectivity, as described in ref 24. The ACF spectrum gives a thickness of 178.1 nm ± 0.2 nm.

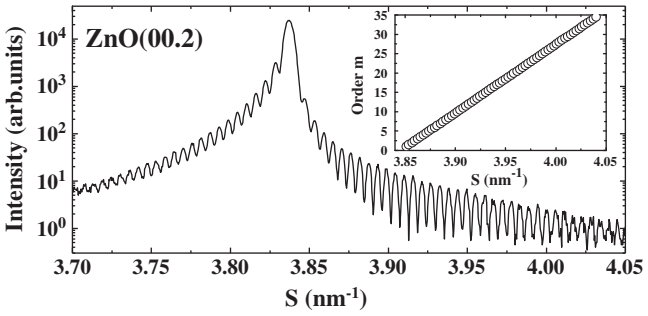


**Fig. 2.** Longitudinal scan of the (00.2) Bragg reflection, showing fringes corresponding to a thickness of 177.5 nm ± 0.5 nm, which was estimated by plotting the fringe order as a function of the fringe position (inset). It is noticeable that the longitudinal scan profiles are similar when measured along the resolution-limited component and when measured just off the specular condition, at the peak of the diffuse scattering.

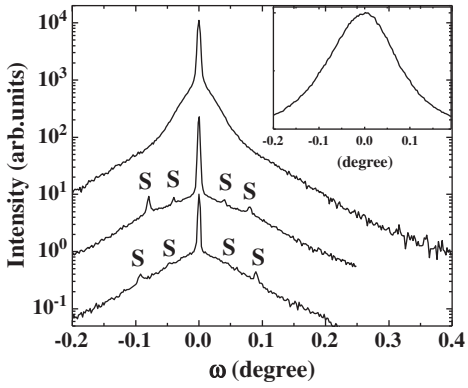


**Fig. 4.** Transverse scans through the (00.2) diffraction peak from 3 thin ZnO layers with different thicknesses: from bottom to top: 70 nm, 150 nm and 1000 nm. Inset: ω rocking curve (open-detector) for the (00.2) peak of the 1000 nm-thick sample.

The asymmetric shape of the diffraction peak, however, suggests that there may be slight inhomogeneous strain along the growth direction.

Fig. 3 shows transverse scans for the (00.2), (00.4) and (00.6) reflections performed using HRXRD. Both the HR (00.2) and (00.4) scans display two-component line-shapes which are not observed for the higher order (00.6) reflection, and which are not resolved in the conventional "open-detector" scan, as shown in the inset of Fig. 4 (although the "open-detector" scan does not resolve the two contributions, it is clear from the peak shape that two contributions are present). Thus a simple figure for the FWHM of any of these conventional "open-detector" ω rocking-curves scans does not adequately reflect the crystal structure of the layer. Considering the transverse-scans, the very narrow and intense component is visible only in the case of weak disorder, due to an exponential damping with crystal plane displacement, and is, therefore, characteristic of ZnO crystallographic planes with a very regular lattice spacing and good parallelicity, over a relatively large lateral correlation length [12,25]. This means that the plane displacements are bounded in magnitude by the substrate, which acts as a source of structural coherence (due to the epitaxy). The mosaic crystals displaying such an effect are unconventional, in that individual mosaic blocks can scatter X-rays coherently with respect to each other due to the long range order, in spite of the presence of short-range disorder. With increasing film thickness, the sharp component was observed to disappear and the broad component was found to narrow (Fig. 4), as has been reported elsewhere [26].

A similar response (two-component line-shape) has been observed for a range of mosaic thin film materials [12,18,25–31]

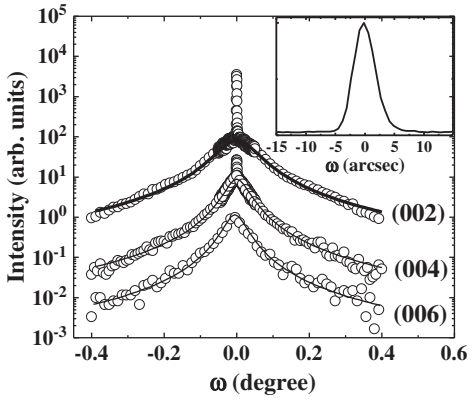


**Fig. 3.** HR transverse scans for the (00.2), (00.4) and (00.6) peaks. The HR (00.2) and the (00.4) reflections exhibit a resolution-limited component. Both the angular shape and the S-shape are different for the 3 reflections. The solid lines correspond to the best fits obtained by Voigt profiles. Inset: detail of the VHR (00.2) narrow component in arcsec.

including other studies on ZnO [32,33]. The narrower "Bragg" peak (with a resolution-limited linewidth) has been attributed to long-range structural correlations, while the broad base has been attributed to diffuse-scattering for shorter-range correlation lengths. The resolution-limited character of the narrower Bragg peak linewidth in HRXRD scans was confirmed through VHRXRD (see inset of Fig. 3), which gave a 5 arcsecs peak width.

Miceli et al. [12,25] developed a phenomenological theory, which explains the broad diffuse-scattering peaks as being defect-induced, and which also accounts for the presence of the narrow component in the line-profiles. In particular, they examined two extreme cases: the case of weak disorder dominated by an effect due uniquely to a lateral defect-correlation-length, $\xi_x$, and the case of strong disorder dominated by strains and giving a mosaic rotational disorder, $\Delta\omega$. Both cases were treated independently and the peak broadening was taken as being either constant in the angular space coordinate if its cause was purely rotational or constant in the reciprocal space coordinate, if it was linked uniquely to a defect-correlation-length. The most common, intermediate, case of the peak broadening depending on a scattering vector in which both effects are combined was treated by N. Herres et al. and L. Kirste et al. who separated the correlation length and mosaicity effects by assuming Gaussian profiles for the transverse scan peaks, in the study of both InAs/GaSb superlattices [34] and (Al)GaN thin layers [35]. It should be noted that these films did not actually display any narrow and intense component, which is most likely due to the higher layer thicknesses employed in the study. The method we propose to separate the correlation length and mosaicity broadening of the transverse-scan diffuse-scattering peak employs assumptions for impacts on the line profile function from each effect.

In powder diffraction, line profile analysis of the ω/2θ Bragg–Brentano diffraction peaks is a well-known method to obtain a measure of both the coherent-domain-size (termed crystallite size) and the micro-strains. Among these techniques, the IB method, using the simulation of the diffraction line-profile through Voigt functions or pseudo-Voigt functions, for instance, provides a rapid and convenient measure of both these parameters. However, compared with powder diffractometry, the case of epitaxial thin films analyses has to be treated differently, since the broadening mechanisms are due to orientation-dependent structural parameters which lead to an anisotropic broadening of the reciprocal lattice points. Therefore, the different broadening mechanisms can be discriminated using ω/2θ and transverse scans.

For the transverse scans, two broadening mechanisms specific to mosaic-thin-films have to be considered: the line broadening caused by the in-plane defect–correlation-length, $\xi_x$, and the mosaicity tilt, $\Delta M$ (giving the mosaicity broadening $\Delta\omega_M$), due to the rotational disorder characteristic of mosaic crystals, resulting in a reflection

broadening of the angular-space coordinates [34]. In the following, since only (00.*l*) surface orientation and transverse-scans on (00.*l*) diffraction planes are considered, broadening due to inhomogeneous strain perpendicular to the sample plane is not taken into account (even for partially relaxed films) since only asymmetric reflections, i.e. where either h or k (or both) Miller index is different from zero, would be affected by such a variation of the strain [34]. As in common powder diffraction, the $\xi_x$ correlation length can be measured using the Scherrer relation [36], applied to the lateral reflection broadening and expressed in terms of the reciprocal space coordinates:

$$\beta_{\xi_x}(S) = \frac{K}{\xi_x} \tag{5}$$

where $\beta_{\xi_x}(S)$ is the IB of the transverse scan diffraction peak due to broadening from the lateral correlation length $\xi_x$ and K is the Scherrer constant (fixed at 1 in the following). In this way, the correlation-length component of the diffuse scattering width is independent of the scattering vector [12]. The mosaicity can be obtained through the following relationship:

$$\beta_M(S) = \Delta M.S_z \tag{6}$$

where $\beta_M(S)$ is the IB due to the mosaicity, expressed in terms of the reciprocal space coordinates. Therefore, the angular width $\frac{\beta_M(S)}{S_z}$ of the diffuse scattering is independent of the scattering vector [12].

The effects of both the mosaicity and correlation length contributions to the observed broadening depend on the shapes of the individual diffraction profiles. Usually, IB methods assume that the constituent profiles are either Cauchy or Gaussian (Williamson-Hall plots). However, Schoening [37] plus Halder and Wagner [22] have shown that the diffraction profile from a particle can be adequately modelled using a Cauchy (Lorentzian) function. In the following, we assume that the average correlation length measured using the Scherrer relation is similar to the average size of the crystallites [35].

Moreover, assuming that the rotational misorientation of the mosaic blocks is randomly distributed, as independent random variates around the surface normal (with a finite variance value) the Central Limit Theorem predicts a Gaussian probability distribution for the mosaic blocks. Thus, a Gaussian shape can be assumed for the mosaicity-induced broadening of the reflection. One has to mention that the existence of preferential tilt angles instead of random rotational misorientation should induce "shoulders" on the narrow Bragg peak [38]. Therefore, a better representation of the experimental profile is given either by a convolution of both Cauchy and Gaussian functions [39,40] (Voigt functions) or by a linear combination of these functions (pseudo-Voigt functions) [41]. Halder and Wagner [22] have shown that an approximation to the IB of a Voigt function is given by a parabolic equation (to an accuracy within about 5%):

$$\beta^2(s) = \beta_{Cauchy}(S).\beta(s) + {\beta_{Gauss}}^2(S) \tag{7}$$

with $\beta(s)$being the measured transverse scan IB, in our case. Then, this equation allows a separation of both effects, using (5) and (6), i.e. from lateral correlation length and mosaicity. Therefore, by employing Eqs. (5) and (6), Eq. (7) can be written, as the following fundamental equation:

$$\left(\frac{\beta(s)}{S_z}\right)^2 = \Delta M^2 + \frac{1}{\xi_x}\frac{\beta(s)}{S_z^2} \tag{8}$$

Therefore, the slope of $\left(\frac{\beta(s)}{S_z}\right)^2$ as a function of $\frac{\beta(s)}{S_z^2}$yields the Cauchy component due to the correlation length, $\xi_x$, and the intercept gives $\Delta M$. In the following, this plot will be called the "Williamson–Hall"-like plot (WHL plot). Fig. 5 shows the WHL plot from the symmetric transverse scans shown in Fig. 3. Each transverse scan has been fitted with two Voigt functions, one for the resolution-limited narrow-component and the other for the broader component. Table 1 summarizes the input data for the WHL evaluation applied to the broad component. From the relation (8) applied to the broad diffuse component in the (00.2), (00.4) and (00.6) peaks (Fig. 5), the correlation length parallel to the surface, $\xi_x$, is 110 nm ± 9 nm and the mosaicity, $\Delta\omega$, is 0.063 ± 0.005°.

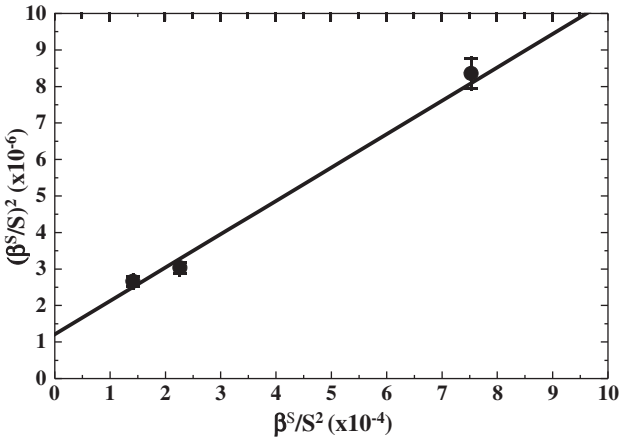


**Fig. 5.** Analyses of the line-broadening of the diffuse scattering transverse scans, using WHL plots.

The longitudinal ω/2θ scans are similar when measured either along the resolution-limited component or just off the specular condition (near the peak of the diffuse scattering). Indeed, these ω/2θ curves (not shown here) display exactly the same shape, multiplied by a constant. Therefore, to explain the limited lateral correlation length, defects originating at the substrate surface, which have an effect only along the growth direction, can be invoked. Similar two-component line shapes from transverse scans have been reported in studies for a variety of thin epitaxial films and have been attributed either to threading dislocations [30,42] and/or misfit dislocations [12,25,30,43] which accommodate the lattice-mismatch at the interface film-substrate, or strain fields due to imperfect stacking faults [44]. In our case, highly localized strain fields, due to planar defects, are unlikely since this would have lowered the correlation length along the growth direction and should have entailed a vertical strain distribution. This was not observed. Thus, it is likely that the defects responsible of the finite correlation-length, are either misfit or threading dislocations. It should be noted that many reports affirm that misfit dislocations are the main source of such two-component transverse-scans line-shapes [30] since the densities of misfit dislocations are much larger, in the relaxed heterostructures, and, should thus have a stronger effect on the peak widths. However, it has also been reported that, while misfit dislocations actually dominate in the diffraction peaks of thin films, threading dislocations become important when thickness increases [42]. In our case, since film thickness is several tens of nanometers, more structural analysis experiments such as Transmission Electron Microscopy are necessary

**Table 1**
Experimentally observed peak positions and peak broadenings of the ZnO (00.*l*) reflections.

| | Peak position | | Peak broadening | |
|---|---|---|---|---|
| Reflection hk.l | 2θ (°) | $S_z$ (nm$^{-1}$) | β(ω) (°) | $\beta_x(S)$ (nm$^{-1}$) |
| 00.1 | 34.3883 | 3.8377 | 0.1657 | 0.0111 |
| 00.2 | 72.4842 | 7.6751 | 0.1001 | 0.0134 |
| 00.3 | 124.9536 | 11.5130 | 0.0939 | 0.0189 |

to determine whether the structural defects reducing the lateral correlation length measured by X-Ray scattering are either threading and/or misfit dislocations. Finally, careful inspection of the (00.2) transverse scans from two other ZnO samples, 150-nm and 70-nm thick, respectively (Fig. 4) reveal satellite peaks (S). Such satellite peaks are characteristic of either misfit/threading dislocations (which may arrange periodically in order to reduce their elastic energy [30]) or a periodical distortion at the ZnO–c-$Al_2O_3$ interface (which may arise if the substrate surface is miscut so that it forms regular terrace [18]). To differentiate between these possibilities, transverse scans were performed for different azimuthal values around the [001] axis. Since the transverse scans display the satellite peaks for azimuthal angles of both 0° (along the [1 0.0] direction) and 90° (along the [1 2.0] direction), such satellite peaks cannot arise from a miscut and are, therefore, more likely to be a characteristic of misfit/threading dislocations. It should be noted that the satellite positions vary slightly with the azimuth angle. Thus the positions of the satellites may correspond to a mean spacing related to a periodic arrangement of misfit or threading dislocations. This periodicity is well-defined (as revealed by the satellite sharpness) at 190 nm, for an azimuthal angle of 0°, and 235 nm, for an azimuthal angle of 90°, for the 150 nm-thick sample. For the 70 nm-thick sample it was smaller (165 nm for an azimuthal angle of 0°). It is possible that the differences between the periodicities in the samples is mainly due to slight differences in the growth conditions rather than the different thicknesses. The relatively high value of the periodicity, and the azimuthal angles where it has been observed, are not evident in the context of the large lattice mismatch between the ZnO and the c-$Al_2O_3$.

## 4. Conclusion

In summary, this paper presented an analysis of the interpretation two components observed in HR X-ray scattering ω transverse scans of PLD-made mosaic ZnO thin films on c-$Al_2O_3$ substrates. The narrower, resolution-limited, peak, was interpreted as characteristic of long-range correlation, and the broader peak, was attributed to defect-related diffuse-scattering resulting in a limited transverse structural correlation length. Thus, the conventional “open detector” ω rocking curve linewidth was found to be ill adapted as an overall figure-of-merit for the structural quality for such mosaic films, in that these different contributions were not meaningfully represented. A WHL IB metric for the HR (00.*l*) transverse-scans was developed as a reliable, fast, accurate and robust alternative. Thus, it was proposed that this would be a better approach for routine non-destructive testing of various mosaic thin film systems including (00.1)-oriented wurtzite materials (such as ZnO and GaN) and (001)-oriented zinc-blende materials (such as GaP and InAs).

A WHL plot method was applied to the diffuse component in the transverse scans for our ZnO films. It gave an average value for the defect lateral correlation-length of 110 nm ± 9 nm for a typical layer. It was deduced from the presence of satellite peaks in transverse scans for films of various thicknesses that this finite lateral correlation length may arise from misfit and/or threading dislocations which exhibit some periodic ordering to accommodate the lattice-mismatch at the film-substrate interface.

## References


[1] R. Triboulet, Proc. SPIE 4412 (2001) 1.
[2] Ü. Özgür, Ya.I. Alivov, C. Liu, A. Teke, M.A. Reshchikov, S. Dogan, V. Avrutin, S.-J. Cho, H. Morkoç, J. Appl. Phys. 98 (2005) 041301.
[3] K. Minegishi, Y. Kowai, Y. Kikuchi, K. Yano, M. Kasuga, A. Shimizu, Jpn. J. Appl. Phys. 36 (1997) L1453.
[4] M. Joseph, H. Tabata, T. Kawai, Jpn. J. Appl. Phys. 38 (1999) L1205.
[5] Y.R. Ryu, S. Zhu, D.C. Look, J.M. Wrobel, H.M. Jeong, H.W. White, J. Cryst. Growth 216 (2000) 330.
[6] D.C. Look, D.C. Reynolds, C.W. Litton, R.L. Jones, D.B. Eason, G. Cantwell, Appl. Phys. Lett. 81 (2002) 1830.
[7] K.-K. Kim, H.-S. Kim, D.-K. Hwang, J.-H. Lim, S.-J. Park, Appl. Phys. Lett. 83 (2003) 63.
[8] D.C. Look, B. Claflin, Y.I. Alivov, S.J. Park, Phys. Status Solidi A-Appl. Res. 201 (2004) 2203.
[9] N. Li, E.-H. Park, Y. Huang, S. Wang, A. Valencia, B. Nemeth, J. Nause, I. Ferguson, Proc. SPIE 6337 (2006) 63370Z.
[10] D.J. Rogers, F. Hosseini Teherani, A. Ougazzaden, S. Gautier, L. Divay, A. Lusson, O. Durand, F. Wyczisk, G. Garry, T. Monteiro, M.R. Correira, M. Peres, A. Neves, D. McGrouther, J.N. Chapman, M. Razeghi, Appl. Phys. Lett. 91 (2007) 071120.
[11] C.G. Darwin, Philos. Mag. 43 (1922) 800.
[12] P.F. Miceli, C.J. Palmstrom, Phys. Rev. B 51 (1995) 5506.
[13] D.J. Rogers, F. Hosseini Téherani, A. Yasan, R. McClintock, K. Mayes, S.R. Darvish, P. Kung, M. Razeghi, G. Garry, Proc. SPIE 5732 (2005) 412.
[14] A.R. Stokes, Proc. Phys. Soc. London 61 (1948) 382.
[15] A.J.C. Wilson, Mathematical Theory of X-Ray Powder Diffractometry, Centrex, Eindhoven, Netherlands, 1963.
[16] A.J.C. Wilson, Nature 193 (1962) 568.
[17] A. Boulle, R. Guinebretière, A. Dauger, J. Phys. D : Appl. Phys. 38 (2005) 3907.
[18] A. Gibaud, R.A. Cowley, D.F. McMorrow, R.C.C. Ward, M.R. Wells, Phys. Rev. B 48 (1993) 14463.
[19] H.P. Klug, L.E. Alexander, 2nd ed, John Wiley, New-York, 1974, p. 618.
[20] D. Balzar, S. Popović, J. Appl. Crystallogr. 29 (1996) 16.
[21] J. Ian Langford, D. Louër, Rep. Prog. Phys. 59 (1996) 131.
[22] N.C. Halder, C.N.J. Wagner, Acta Crystallogr. 20 (1966) 312.
[23] O. Durand, D. Rogers, F. Hosseini Teherani, M. Andrieux, M. Modreanu, Thin Solid Films 515 (2007) 6360.
[24] O. Durand, Thin Solid Films 450 (2004) 51.
[25] P.F. Miceli, J. Weatherwax, T. Krentsel, C.J. Palmstrøm, Physica B 221 (1996) 230.
[26] M. Becht, F. Wang, J.G. Wen, T. Morishita, J. Cryst. Growth 170 (1997) 799.
[27] P.M. Reimer, H. Zabel, C.P. Flynn, J.A. Dura, Phys. Rev. B 45 (1992) 11426.
[28] M. Huth, C.P. Flynn, Appl. Phys. Lett. 71 (1997) 2468.
[29] G.L. Zhou, C.P. Flynn, Phys. Rev B 59 (1999) 7860.
[30] V.M. Kanager, O. Brandt, H. Riechert, K.K. Saberfeld, Phys. Rev. B 80 (2009) 033306.
[31] A. Boulle, R. Guinebretière, A. Dauger, J. Phys. D: Appl. Phys. 38 (2005) 3907.
[32] Y.F. Chen, H.J. Ko, S.K. Hong, K. Inaba, Y. Segawa, T. Yao, J. Cryst. Growth 227–228 (2001) 917.
[33] T.-B. Hur, Y.-H. Hwang, H.-K. Kim, H.-L. Park, J. Appl. Phys. 96 (2004) 1740.
[34] N. Herres, F. Fuchs, J. Schmitz, K.M. Pavlov, J. Wagner, J.D. Ralston, P. Koidl, C. Cadaleta, G. Scamarcio, Phys. Rev. B 53 (1996) 15688.
[35] L. Kirste, K.M. Pavlov, S.T. Mudie, V.I. Punegov, N. Herres, J. Appl. Crystallogr. 38 (2005) 183.
[36] P. Scherrer Nachr, Gött 2 (1918) 98.
[37] F.R.L. Schoening, Acta Crystallogr. 18 (1965) 975.
[38] F. Conchon, A. Boulle, R. Guinebretiere, E. Dooruhée, J.-L. Hodeau, C. Girardot, S. Pignard, J. Kreisel, F. Weiss, L. Libralesso, T.L. Lee, J. Appl. Phys. 103 (2010) 123501.
[39] H. De Th, J.I. Keijser, E.J. Langford, A.B.P. Vogels Mittemeijer, J. Appl. Crystallogr. 15 (1982) 308.
[40] J.I. Langford, Proceedings of the international conference Accuracy in Powder diffraction II, 1992, p. 110.
[41] R.A. Young, D.B. Wiles, J. Appl. Crystallogr. 15 (1982) 430.
[42] V.M. Kanager, R. Köhler, M. Schidbauer, R. Opitz, B. Jenichen, Phys. Rev. B 55 (1997) 1793.
[43] R.I. Barabash, W. Donner, H. Bosch, Appl. Phys. Lett. 78 (2001) 443.
[44] A. Boulle, R. Guinebretière, A. Dauger, J. Appl. Phys. 97 (2005) 073503.